Ignus 2.0 Engine Overview

The Students for the Development and Exploration of Space at the University of California, San Diego (SEDS UCSD) has developed their fourth additively manufactured liquid propellant engine. The purpose of the project is improve on the design of the *Ignus 1.0* engine, SEDS UCSD's second additively manufactured engine. The design process for the Ignus 2.0 engine is discussed and justified through calculations, CAD, simulations, and iterative analysis. The benefits of additive manufacturing allows for more rapid and efficient development, in terms of lead time and cost compared to traditional subtractive manufacturing. The Ignus 2 attempts to close the iterative design loop with rapid prototyping enabled via the 3D printing technology.

Nomenclature

P_c - Chamber pressure
$\dot{m}_f$ - Fuel mass flow rate
$\dot{m}_o$ - Oxidizer mass flow rate

O/F - Mass flow rate ratio / Mixture ratio
t_{burn} - Burn time
D_c - Chamber diameter
B - Initial contraction angle
R_2 - Initial contraction radius
R_1 - Throat contraction radius
L* - Characteristic length
L_c - Chamber length
L_{cyl} - Cylindrical chamber length
D_t - Throat diameter
R_n - Initial throat expansion radius
T_n - Initial throat expansion angle
L_e - Nozzle exit length
T_e - Final nozzle expansion angle
D_e - Exit diameter
L - Total nozzle length (L_c+L_e)
A_e/A_t - Contraction ratio
L_e/D_t - Expansion ratio
LOX - Liquid oxygen
P_{amb} - Ambient Pressure (14.7 psia)
ρ - Fluid density

Introduction

In the new advanced era of space exploration, the technology to produce and reuse flight vehicle hardware such as propulsion systems has dramatically made space more accessible and affordable. Considering the long lead times for traditional manufacturing, the high cost associated with the fabrication, and limited funding to pursue projects related to the advancement of space technology and exploration, the additively manufacturing approach has revolutionized the engineering approach to such problems. In addition, it has also made the development of rocket engines more accessible and thus has allowed for more opportunities for engineers to expand their creativity and provide more useful research for the aerospace industry.

Designing and testing rocket engines is one of the most complex systems to develop in the field of engineering due to the extreme temperatures, pressures, tolerances, and usage of volatile propellants. The additive manufacturing technology allows companies and even undergraduate students to design and research rocket engines without being bound by the limitations of cost, lead times, quality control, and reusability.

For the Ignus 2.0 engine, we explore the design improvements that we are able to implement on the Ignus 1.0 engine and scale up the performance due to the versatility of additive manufacturing.

Design Approach

The design of Ignus 2.0 follows the same initial approach as the Ignus 1.0 engine. To begin the design process of the liquid engine, we evaluate our design parameters to be the obtainable mass flow rates and chamber pressure. We input these parameters into Rocket Propulsion Analysis (RPA), a software tool used to determine the chamber geometry as well as expected combustion and propellant data. We then export the chamber geometry DXF from the software and expand our chamber design upon it. The RPA parameters are shown as follows:

Engine Parameters	
● *Ignus 1.0* ○ $P_c = 375\ psi$ ○ $\dot{m}_f$ = 0.834 lbm/s ○ $\dot{m}_o$ = 2.06 lbm/s ○ O/F = 2.47 ○ Thrust = 750 lbf ○ t_{burn} = 6.67s ○ LOX/RP-1, Partially Blow-Down ○ 3D Printed Inconel 718	● *Ignus 2.0* ○ $P_c = 500\ psi$ ○ $\dot{m}_f$ = 0.966 lbm/s ○ $\dot{m}_o$ = 2.340 lbm/s ○ O/F = 2.42 ○ Thrust = 830 lbf ○ t_{burn} = 11.0s ○ LOX/RP-1, Pressure Fed ○ 3D Printed Inconel 718 ○ Improved performance and efficiency

***Rocket Propulsion Analysis* Input Data**

Initial Data		
Engine Definition	***Nozzle Flow Model***	
● Chamber Pressure: 500 psi ● Mass Flow Rate: 3.20 lbm/s ***Propellant Specification*** ● Optimum Mixture Ratio for max delivered I_{sp} ● Oxidizer: $O_{2\ (l)}$ ● Fuel: RP-1 ***Ambient Condition / Throttle Settings*** ● Fixed ambient pressure: 1 atm	***Nozzle Conditions*** Contraction area ratio A_c/A_t: 14.743 *Nozzle Exit Condition* ● *Pressure: 1 atm (Sea Level)* *Frozen Equilibrium Flow enabled* ● Freezing at the area ratio A_{fr}/A_t: 1 ***Nozzle Shape and Efficiencies*** *Reaction Efficiency* ● Estimate the efficiency on the basis of defined engine parameters *enabled*	*Nozzle shape and Efficiency* ● Bell Nozzle ● Estimate the efficiency for length 80% on the basis of defined nozzle exit condition *enable* *Nozzle Flow Effects* ● Consider: 1. Multiphase flow and phase transition effects 2. Species ionization effects ● Estimate performance loss

		due to flow separation in overexpanded nozzle

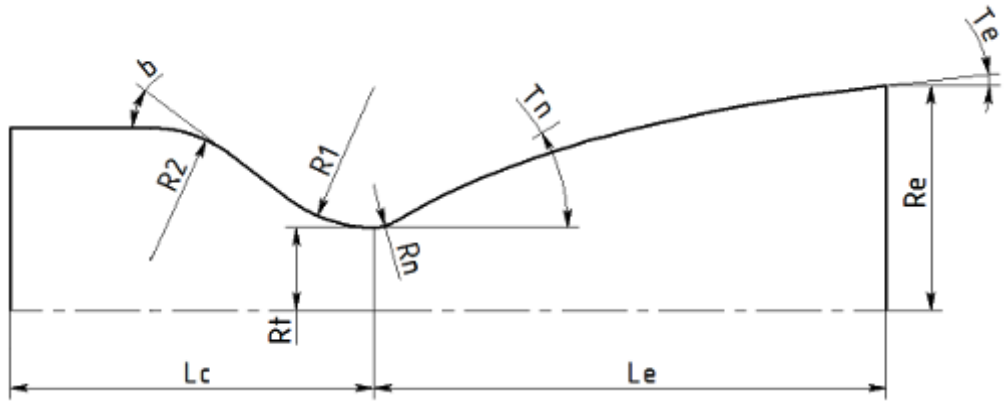

Figure 1 - Converging-Diverging Nozzle Contour

Thrust Chamber Size and Geometry			
Thrust and Mass Flow Rates		*Geometry of thrust chamber with parabolic nozzle*	
• Chamber thrust (vac): 917.45894 lbf • Specific impulse (vac): 286.70592 s • Chamber thrust (opt): 828.79465 lbf • Specific impulse (opt): 258.99833 s	• Total mass flow rate: 3.200 lbm/s • Oxidizer mass flow rate: 2.23386 lbm/s • Fuel mass flow rate: 0.96614 lbm/s • Divergence efficiency: 0.99106 • Drag efficiency: 0.96462 • Thrust coefficient: 1.60152 (vac)	D_c = 5.09 in b = 30.00° R_2 = 6.53 in R_1 = 0.99 in L* = 60.08 in L_c = 6.25 in L_{cyl} = 1.44 in	D_t = 1.21 in R_n = 0.23 in, T_n = 16.67° L_e = 2.70 in, T_e = 14.95° D_e = 2.74° L = 8.95 in A_e/A_t = 5.14 L_e/D_t = 2.23

Injector Plate

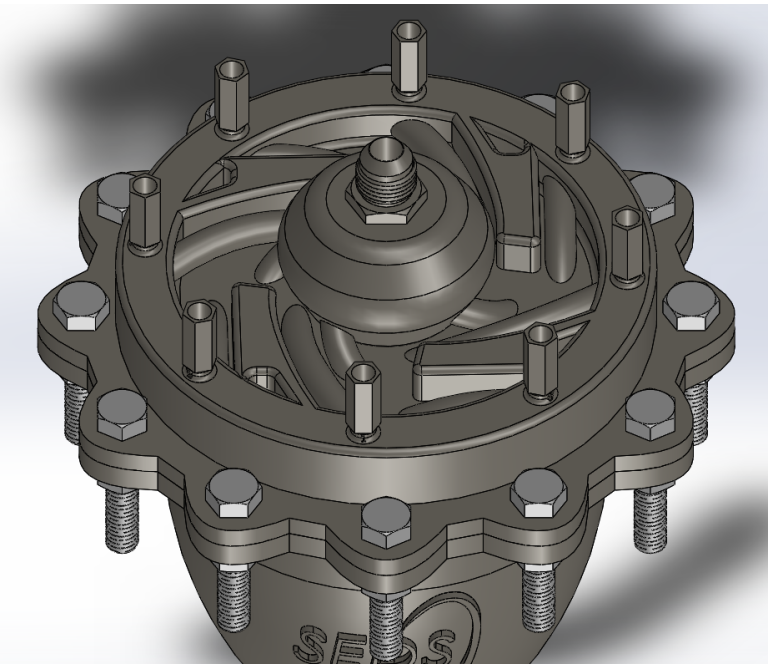

Figure 2 - Ignus 2.0 Injector Plate

Like-on-Like Impingement

The injector plate is designed to deliver the RP-1 fuel and LOX to the combustion chamber through like-on-like impingement similar to the Ignus 1 engine. This impingement design was chosen due to its high reliability, hardware compatibility, and relatively easy manifolding and manufacturing[1]. A MATLAB script was written to take engine parameters as inputs and output results that yield the required amount of orifices and their sizes for the injector plate. Given the mass flow rate ṁ (lb/s), propellant density ρ (lb/ft^3), and a factor for the head-loss coefficient K, the injection area (in^2) and orifice diameters (in) for both fuel and oxidizer orifices are calculated using the following equations from Huzel and Huang[2]:

$$A_{inj} = \dot{m}\sqrt{\frac{2.238\,K}{\rho\,\Delta P}}$$

$$d_{orifice} = \left(\frac{3.627\,K\,\dot{m}}{\rho\,\Delta P\,N^2}\right)^{0.25}$$

The injector face pattern design is similar to the Ignus 1.0 engine, with slight adjustments due to the difference in mass flow rates and design chamber pressures. For symmetry, the ratio of LOX to RP-1 orifices was chosen to be 2:1.

The RP-1 fuel injection spray is designed to have N = 24 orifices,

$$d_{orifice} = \left(\frac{3.627\ (1.2)\ \ (0.96614)}{(56.8)(0.30*500)\ (24)^2}\right)^{0.25}$$

$$d_{orifice} = 0.0304”$$

The LOX injection spray is designed to have N = 48 orifices,

[1] Gill, G. S., and W. H. Nurrick. *Liquid Rocket Engine Injectors*. NASA SP-8089, 1976.

[2] *Modern Engineering for Design of Liquid-Propellant Rocket Engines*. Huzel and Huang (p. 115). 1992.

$$d_{orifice} = \left(\frac{3.627\ (1.2)\ (2.3386)}{(71.23)(0.30*500)\ (48)^2}\right)^{0.25}$$

$$d_{orifice} = 0.0254"$$

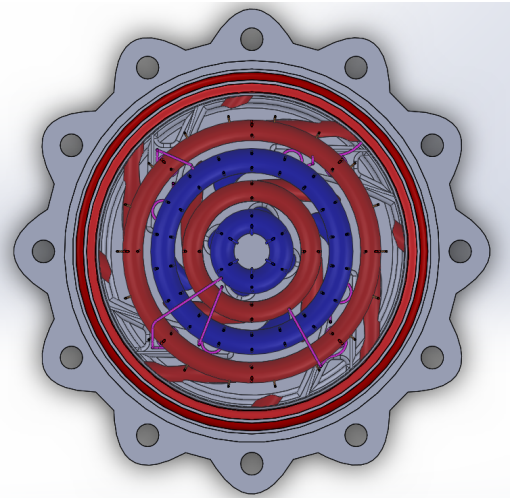

Figure 3 - Transparent view of injector face

In consideration of the orifice shrinkage of the Inconel 718 during additive manufacturing, the CAD orifices diameters are increased by 0.01" according to Atyam & Sojk3a

A head loss coefficient of K = 1.2 was used as the orifices are designed to be filleted at the entrance for minimal head loss. The filleted entrances provide the lowest $\Delta P$and the best stream control. The design parameter used for filleting the entrances satisfy the following equation:

$$\frac{R}{d} > 0.3$$

where R is the radius of the fillet and d is the diameter of the orifice[3].

The primary impingement angles of the injection elements are designed to be $\alpha = 60°$, as it is experimentally found to produce acceptable backsplash characteristics[4]. The spacing between the injection elements is designed to provide an impingement distance that is between 5-7 times the orifice diameter[5]:

$$d_{imp} \leq 7d_{orifice} \text{ and } d_{imp} \geq 5d_{orifice}$$

Therefore, an impingement distance d_{imp} of 6 times the orifice diameter was chosen as the design parameter to determine the spacing between the injection elements:

$$d_{imp} = 6\, d_{orifice}$$

For RP-1 fuel,

$$d_{imp} = 6\ (0.0304)$$

$$d_{imp} = 0.1824"$$

For LOX,

$$d_{imp} = 6\ (0.0254)$$

$$d_{imp} = 0.1524"$$

The impingement of the elements are designed such that the inner and outer elements inject towards the elements in between for uniform mixing.

---

[3] Gill, G. S., and W. H. Nurrick. *Liquid Rocket Engine Injectors*. NASA SP-8089, 1976.

[4] Gill, G. S., and W. H. Nurrick. *Liquid Rocket Engine Injectors*. NASA SP-8089, 1976.

[5] Gill, G. S., and W. H. Nurrick. *Liquid Rocket Engine Injectors*. NASA SP-8089, 1976.

To obtain the spacing between the injection elements, we use the following trigonometric relation:

$$sin(\frac{\alpha}{2}) = \frac{l_{separation}}{2\,d_{imp}}$$

$$l_{separation} = 2\,d_{imp} sin(\frac{\alpha}{2})$$

For LOX,

$$l_{LOX,\,separation} = 2\,(0.1524)\,sin(30°)$$

$$l_{LOX,\,separation} = 0.152”$$

For RP-1 fuel,

$$l_{RP1,\,separation} = 2(0.1824)\,sin(30°)$$

$$l_{RP1,\,separation} = 0.182”$$

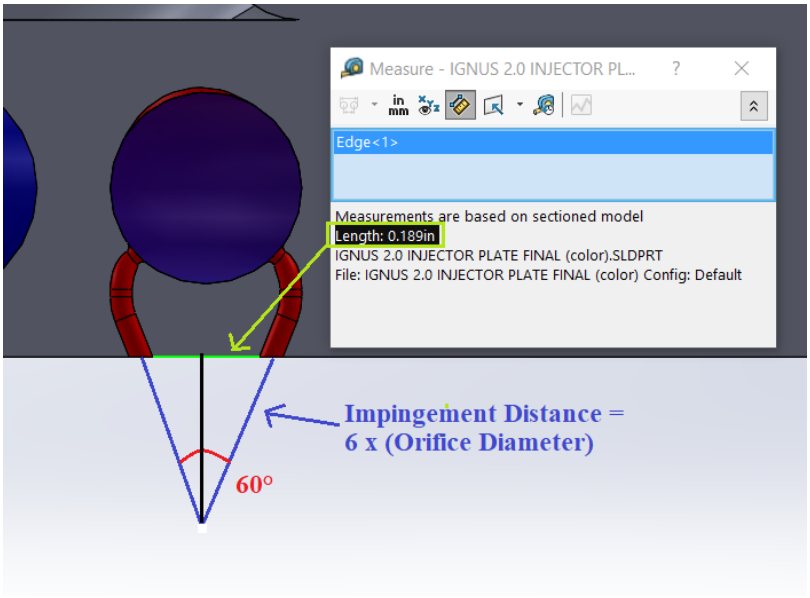

Figure 4 - Separation distance for RP-1 injection elements

External Manifold

The fuel is delivered to the injector plate from the regenerative cooling channels along the contour of the nozzle. The fuel annulus is symmetric about the origin and delivers the fuel to the internal manifold.

The LOX collection chamber was redesigned from Ignus 1.0 to fit the parameters of the Ignus 2.0 engine. The distribution lines from the LOX chamber and the RP1 annulus were resized according to the mass flow rate of the engine.

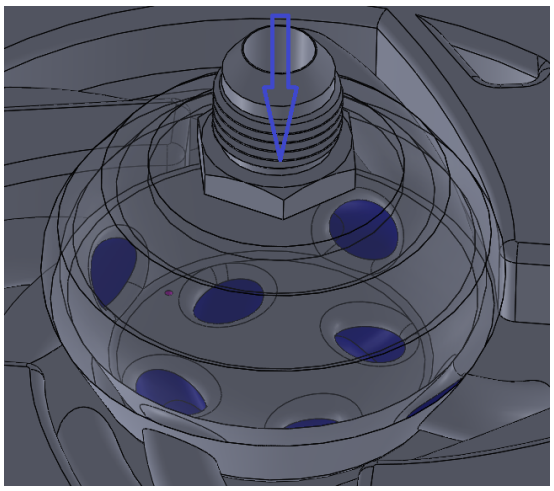

Figure 5 - Transparent view of LOX Dome

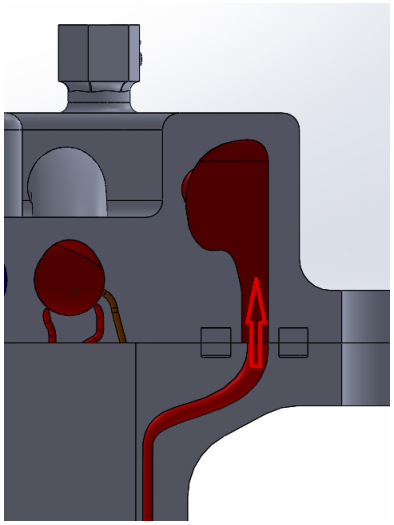

Figure 6 - RP1 Annulus

The arrows on Figure 5 and Figure 6 represent the flow of the LOX and RP1 to the LOX dome and RP1 annulus, respectively.

Internal Manifold

The internal manifold consists of four (4) propellant rings that deliver the propellant to the injector face before main combustion. Similar to the Ignus 1 design, the rings alternate in propellant, with the fuel rings on the outermost and second inner ring and with the oxidizer rings placed closest to the centerline and second furthest from the wall. This arrangement ensures that the fuel from the outermost ring would be closest to the chamber wall, assisting with the chamber wall cooling and prolonging hardware durability. Having more of the oxidizer slightly inboard results in the core elements providing a higher degree of mixing uniformity and outer elements yielding a gradient in mixing from fuel-rich nearest to the wall and oxidizer-rich near the core elements[6].

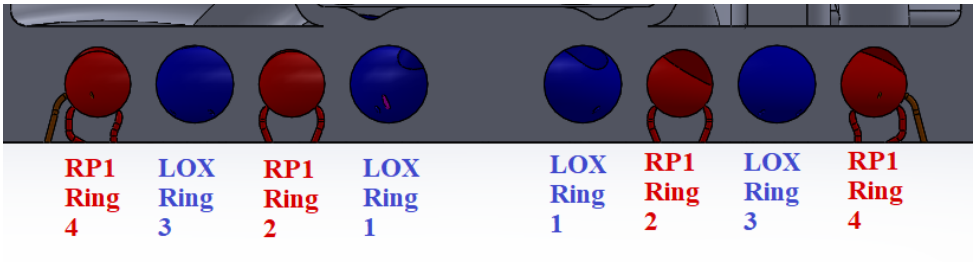

Figure 7 - Distribution Rings

The manifolds are designed to provide efficient distribution while also compromising flow area volume. Each manifold is designed such that the velocity head (dynamic component of the total pressure) does not exceed 1% of the local system pressure[7]. For this design, a chamber pressure of 500 psia and a 30% ΔPacross the injector yield a local system pressure of 650 psia dictates that the velocity head in the feed line should not exceed $H_{vel} \leq$ 6.5 psia. The velocity head is calculated as follows:

$$H_{vel} \geq \frac{2.238\ \dot{m}}{\rho\ A^2}$$

For a circular cross sectional flow area, $A = \pi \frac{d^2}{4}$, the minimum diameter of each ring is calculated to agree with this design standard:

$$d \geq \sqrt[4]{\frac{8.952\ \dot{m}}{\pi\ \rho\ H_{vel}}}$$

For RP-1 fuel,

$$d \geq \sqrt[4]{\frac{8.952\ (0.96614)}{(56.8)\ (6.5)\ \pi}}$$

$$d \geq 0.294"$$

For LOX,

$$d \geq \sqrt[4]{\frac{8.952\ (2.3386)}{(71.23)\ (6.5)\ \pi}}$$

[6] *Liquid Rocket Engine Injectors, NASA SP-8089*. Mar 1976.

[7] *Modern Engineering for Design of Liquid-Propellant Rocket Engines*. Huzel and Huang (p. 115). 1992.

$$d \geq 0.346"$$

Structural Components

The injector plate will be 3D printed separately from the combustion chamber and will be connected using 12 fully T6-*+87 threaded ⅜" bolts. The reduction in the number of bolts, increase in bolt size, and the floral design pattern of the bolt arrangement allow for easier assembly while also retaining the required structural compatibility the engine requires.

Under nominal conditions the engine will operate at a chamber pressure between 450 psi and 500 psi. If the injector plate exposed to engine conditions is approximated as a circle of diameter 5.09" neglecting the injection elements, it has a surface area

$$A_{plate} = \frac{\Pi}{4} D^2$$

$$A_{plate} = \frac{\Pi}{4}(5.09^2)$$

$$A_{plate} = 20.35\ in^2$$

To find the force on the plate, F_{plate}, the chamber pressure P_c is multiplied by A_{plate}:

$$F_{plate} = P_c * A_{plate}$$

$$F_{plate} = 500\ psi\ *\ 20.35\ in^2$$

$$F_{plate} = 10175\ \text{lbf}$$

Assuming that the load is distributed evenly between bolts, each will have to support $\frac{10175\ lbf}{12} = 847.92 lbf \approx 850\ lbf$.

In order to determine the factor of safety required for the bolts, hard start data from our previous engine, Ignus 1, were used. During the Ignus 1 hard start, chamber pressure values of roughly 450 psi were implied from measured values of output thrust. Unfortunately, the PTs were unable to take pressure data due to the short duration of the hard start event. A chamber pressure of 450 psi occurring in an engine with nominal chamber pressure of 375 psi means a 20% increase over nominal pressure. In our engine operating at 500 psi, a 20% increase above nominal would lead to a chamber pressure of 600 psi. However, due to a lack of a more rigorous analysis of the pressures that could be produced during a hard start and the capability of our bolts and other structural components, we can be cautious and place an upper bound on hard start pressures at 2000 psi. Repeating the above calculations but with a chamber pressure of 2000 psi, we find the amount of force that each bolt needs to be preloaded to, $F_{preload}$, is 3400 lbf. For our purposes the preload on the bolts should be able to provide 100% of the support that we need.

Using the following equation:

$$T_{app.} = F_{preload}\, KD$$

where $T_{app.}$ (lbf-ft) is the torque required to be applied to the bolt to produce $F_{preload}$ *(lbf)*, *K* is the unitless thread factor, and *D* is the shank diameter (in.), T_{app} can be calculated. In this analysis, *K* is assumed to be 0.2, the upper end of unlubricated thread factors selected to err on the side of caution. D will be taken as ⅜" even though our particular bolts are fully threaded and do not have shanks.

$$T_{app.} = 3400\ lbf\ *\ 0.2\ *\ \frac{\frac{3}{8}}{12}$$

$$T_{app.} = 21.25\ lbf - ft.$$

Next, the force required to cause shearing of the threads will be calculated,

$$F_{pullout} = 0.4\pi DL_{eng}\tau_u.$$

$L_{eng.}$ *(in.)* represents the thread engagement length, or the length of the bolt which makes contact with the nut, taken to be the entire length of the nut: $\frac{21}{64}$". τ_u can be approximated by the equation $\tau_u \approx \frac{\sigma_u}{\sqrt{3}}$, meaning that it is roughly 60% of the tensile strength of the bolt, an estimate recommended by the Industrial Fastener Institute[8] . The ultimate tensile strength of the bolt provided by the manufacturer is 130,000 psi. Therefore, $\tau_u \approx \frac{130{,}000\ psi}{\sqrt{3}} = 75{,}060\ psi.$ We calculate that

$$F_{pullout} = 0.4 * \pi * 10\backslash * \frac{21}{64} * 75060\ psi$$

$$40.,mn\ bvF_{/.mbvc,/pullout} = 11600\ \text{lbf}$$

This means that each bolt can support over 11,000 lbf load before failing, well above the preload force that each bolt is loaded to. The nuts and bolts selected to couple our injector system to the combustion chamber have very similar hardness values and thus will not damage each other significantly once threaded. Some nut deformation is expected because locknuts utilize the deformation of their center threads to provide a better grip on the bolt.

It is also important for us to understand how the injector plate will deform during firing of the engine and the stresses that it will be put under. For the sake of these calculations the plate will be approximated as a circular, pressurized plate with a fixed perimeter. To find the maximum deflection, which should occur at the center of the plate, the following equation will be used:

$$\delta_{max} = \frac{3}{16}\frac{pR^4(1-\nu)}{Et^3}$$

where p is the pressure on the plate (psi), R the radius (in.), ν the unitless poisson ratio of Inconel 718, E is Young's modulus (psi), and t (in.) is the thickness of the plate. *E*and νare taken to be 26,200 ksi and 0.27, respectively[9]. The thickness of the plate is designed to be 0.25", the height of the flange.

$$\delta_{max} = \frac{3}{16} * \frac{500*(2.545)^4*(1-.27)}{(26{,}200*10^3)*(0.25)^3}.$$

$$\delta_{max} = 0.007\ in$$

In practice, the plate is likely to deform less than this, as the injector plate is significantly thicker than 0.25 in. To find the max stress applied on the plate, again at the center, we use the following equation:

$$\sigma_{max} = \frac{3}{4}p\left(\frac{R}{t}\right)^2$$

$$\sigma_{max} = \frac{3}{4} * 500 * \left(\frac{2.545}{0.25}\right)^2$$

$$\sigma_{max} = 38{,}900\ psi$$

A static structural FEA analysis was conducted on the CAD model of our actual injector plate, which will provide a more accurate assessment on how the injector plate will deform under load.

Combustion Chamber

Combustion Stability

[8] Inch Fastener Standards, 7th ed. 2003. B-8

[9] "Inconel Alloy 718". Special Metals.

Similar to the Ignus 1.0 engine, the ratio between the chamber diameter and the exit stream velocity *d/V* will help determine margin for acoustic combustion instability. The Hewitt Plot was used to determine stream velocities that would yield stable combustion and determine allowable orifice diameters. From the required stream velocities, it was decided that the trikes from Ignus 1 were omitted in the design of this engine because low thrust engines such as Ignus 2.0 do not produce high combustion oscillations that require extensive design considerations.

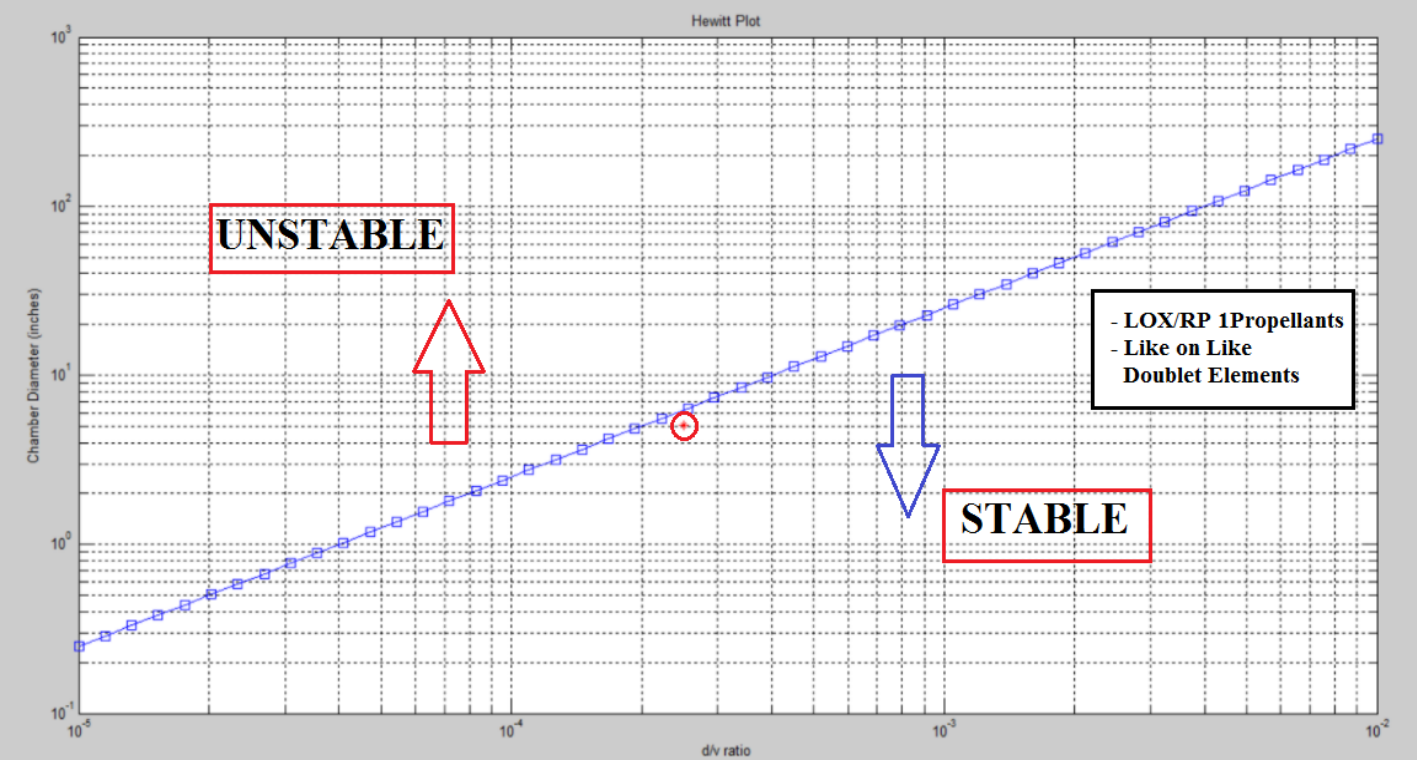

Figure 8 - $\frac{d}{v}$ ratio on Hewitt Plot

A general rule for the Hewitt plot is to have a d/v ratio placed to the right of the curve. Using the chamber diameter from RPA, a d/v ratio of 0.0025 was chosen to calculate the exit stream velocities of each propellant.

Chamber Cooling and Thermal Protection

Due to the extreme temperatures and pressures in an operating engine, any sustained firing will normally melt the hardware in seconds. The design approach for the Ignus 2.0 engine was to ensure that the temperature at any point in the chamber is below 40% of the melting point of the chamber material. This is referred to as creep temperature (CCT) and is approximately 400°C or 700K for Inconel 718, the chamber material of Ignus 2. Engine operations before and during the hot fire exerts cyclic loading on the engine, and keeping the chamber below CCT ensures no deformation and that the mechanical properties of the engine do not alter too much.

The Ignus 2.0 utilizes a coupled cooling method of film and regenerative cooling (regen). The fuel enters the combustion chamber by first flowing through cooling channels inside the wall of the engine. The forced convection of the RP1 encourages heat transfer from the chamber inner wall, thereby keeping the Inconel cool. Due to boundary layer formation on the wall, a thin layer of slow moving gas forms the gas-side boundary layer in the combustion chamber. This acts as an insulating blanket that further shields the heating and lower the temperature. This effect is enhanced by admitting a thin layer of liquid propellant along the gas-side wall, known as film cooling.

Regenerative Cooling

Regenerative (Regen) cooling works by removing heat via forced convection of a coolant on the cool-side of the chamber walls. The coolant is usually a liquid propellant which has a high thermal capacity to absorb the heat. This method is highly efficient as the absorbed heat becomes added enthalpy for the combustion, but comes at the cost of a pressure drop required to push the coolant against viscous friction. In general, the regen channels' geometry may take on 1) co-axial 2) tubular or 3) rectangular cross sections, in order of increasing pressure drop.

When designing regen channels, it is important to keep in mind the operating pressure and temperature within the coolant. Refer to Figure 9, Line A1-A2-A3 represents coolant below critical point, and line B1-B2-B3 represents coolant above critical point. Substances are distinguished clearly between liquid and gas by a vapor dome. Beyond the apex of the dome (the critical point), the distinction becomes ambiguous and substance can exhibit extreme thermophysical properties. This is crucial as cooling predictions depend on the thermophysical properties such as thermal capacity, conductivity, etc.
For the Ignus 2.0 engine, coolant in the regen channels runs above the chamber pressure of 500 psi, which is well above the critical pressure of 315 psi (2.2 MPa) for RP1. Under supercritical condition, no boiling can occur and wall temperature increases continuously with increase in heat flux. It is then crucial to maintain the coolant temperature below the critical temperature of 660K, beyond which "a gradual transition to a stable supercritical vapor-film boundary layer begins". This has the effect of lowering the heat transfer coefficient and coolant heat absorption, and wall quickly heats to failure.

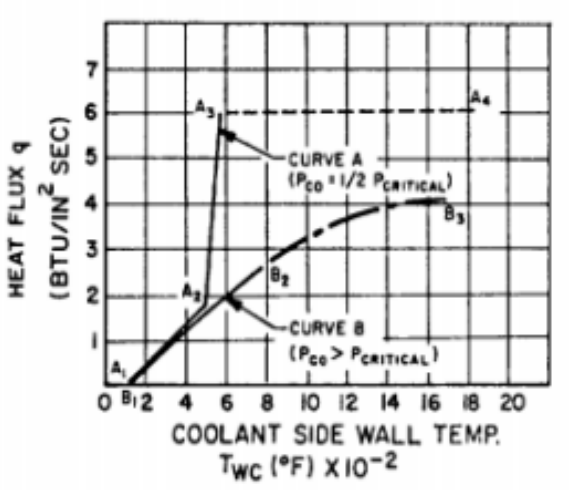

Figure 9 - Heat flux versus coolant side wall temperature of typical propellant in various heat transfer regions

		RP-1	T(S)-1	Methane
Boiling point (1 bar)	K	450-547	466-547	112
Freezing Point	K	224	226	91
Density @ 16 °C	kg/m³	809	836	0.72
Density (liquid) @ boiling point	kg/m³			422.5
Kinematic Viscosity (liquid)	mm²/s	3.02 @ 274 K	4.01 @ 274 K	0.28 @ 111 K
Critical Temp.	K	662	658	190
Critical Pressure	Pa	2 171 848	1 820 000	4 599 200
Specific Heat Capacity	J/(kg K)	2093	1980	3480
Specific Energy	MJ/kg	43.34	43.13	50
Volume specific energy (liquid)	MJ/m³	34 934.14	35 887.02	21 125.00
Coking limit	K	560	?	950
Handling properties		Storable	Storable	Cryogenic
		$CH_{1,952}$	$CH_{1,946}$	CH_4
Molecular mass	kg/kmol	172	167	16.043

Figure 10 - Some basic thermodynamic properties of the two propellant options

The regen cooling efficiency *h* is limited by the pressure drop across the cooling channels (Δ*P*). In order to understand the order of variation between *h* and Δ*P*, a dimensional analysis was performed. The Nusselt number ν [describes the cooling efficiency and is given in the equation below:

$$\nu = C_1 Re^{0.8} P_r^{0.4} \left(\frac{\mu}{\mu_W}\right)^{0.14} = \frac{h_c d}{k}$$

$$Re = \frac{\rho V_{co} d}{\mu}$$

$$P_r = \frac{\mu C_p}{k}$$

where C_1 is a constant (different values for various coolants), *Re* is the Reynolds number, P_r is the Prandtl number, μis the coolant viscosity at bulk temperature, μ_W is the coolant viscosity at coolant sidewall temperature, *d* is the coolant passage hydraulic diameter [in], *k* is the coolant thermal conductivity $\left[\frac{Btu\ in}{s-in^2 °F}\right]$, ρis the coolant density $\left[\frac{lb}{in^3}\right]$, V_{co} is the coolant velocity $\left[\frac{in}{s}\right]$, C_p is the coolant specific heat at constant pressure $\left[\frac{Btu}{lb\ °F}\right]$.

Dimensional analysis yields that $h_{regen} \sim \frac{K}{d^2}$, where K is a constant and $\Delta P \sim \frac{K}{d^5}$. From this analysis, we see that the cooling efficiency is limited by the pressure drop budget. As *h* is dependent on *d*, one may tailor the regen geometry such that the cooling is highest for critical region of heating and lower elsewhere to optimize cooling for the given available Δ*P* budget.

Film Cooling

Film cooling involves admitting a thin layer of liquid coolant, usually the fuel, to the hot-gas side of the chamber wall. The layer, in addition to the hot gas boundary layer, forms an isothermal blanket that is highly effective in lowering the wall temperature. A rough estimate of the film cooling mass flow can be found using the equations:

$$\int_a^b h_g(T_f - T_{sat})\, dA = (\frac{\eta_m}{\eta_g})\, w_{FC}\, (C_p\, \Delta T_{sub} + \Delta H_v)$$

For cylindrical chambers, the result of integration is

$$h_g(T_f - T_{sat})\pi\, D_c\, L$$

We also set T_{wg} equal to T_{sat} in the liquid region and we can conservatively approximate $\frac{\eta_m}{\eta_g}$ to be 0.4. The equation assumes all heat is transferred into the sum of the energy to both heat and boil the film coolant. Some properties of RP-1 at atmospheric and room temperature are shown in appendix 3. Compared to regen cooling, film cooling is a much more complex phenomena and a rigorous analysis is extremely complicated. Its interaction with the hot-gas boundary layer, viscosity, supersonic interactions at the throat and other phenomena presents a highly coupled, nonlinear set of equations that can only be solved with an advanced software package.

When fuel is injected onto the chamber walls, it undergoes heating from the hot combustion gases but also lose heat to the walls and regen coolant, resulting in film coolant evaporation and boiling. At the operating chamber pressure of 500 psi, the coolant experiences supercritical, non-boiling heating. But the static pressure decreases along the CD nozzle and falls below the critical pressure of RP-1 before the throat. At which point, the surface of the film coolant exposed to the hot combustion gas will be well above its saturation temperature, and nucleate boiling will take place. Let's define Phase 1 to be the supercritical heating and Phase 2 to be the non-supercritical phase. The goal of the analysis then, is to find out the optimal film coolant mass flow rate for efficiency and adequate cooling.

A cylindrical shell control volume (CV) is defined on the inner perimeter of the combustion chamber, as shown in green. The CV has radius Rc and spans from x to x+Δx. The shell has infinitesimal thickness, and represents the volume containing the layer of film coolant injected. The coolant element injected into the CV carries an enthalpy at time *t*, and leaves the CV carrying an enthalpy at time t+Δt. In this process, heat is transferred into the coolant element via hot combustion gases by

$$q_c = h_c(T_{aw} - T_{co})$$

but heat is also transferred into the wall and regen coolant by

$$q_w = h_w\,(T_{co} - T_w).$$

The CV then, captures the coupled heat transfer between the hot combustion gas with film coolant and film coolant with regen coolant. What goes in, must come out. The analysis essentially accounts for all energy transaction within the CV.

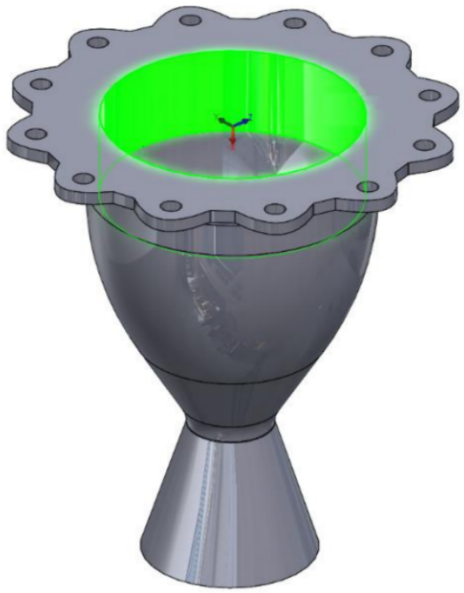

Figure 11 - Cylindrical shell control volume (CV)

The cooling analysis is illustrated as follows. First, the assumptions defined in this analysis are

1) Neglect nucleate boiling / evaporation effects:
2) Neglect viscous interaction of film with the wall:
3) Fluid fills up the CV
4) Steady State

5) Cylindrical CV

The fundamental equations are

$$e_{in} = \rho u C_p T(2\pi r)\Delta r \,|_x$$

$$e_{out} = \rho u C_p T(2\pi r)\Delta r \,|_{x+\Delta x}$$

$$Q_{in} = q_c(2\pi r)\Delta x = h_g A\,(T_{aw} - T_{co})$$

$$Q_{out} = q_w(2\pi r)\Delta x = h_f A\,(T_{co} - T_w)$$

Energy conservation for the system is defined as:

$$e_{in} + Q_{in} = e_{out} + Q_{out}$$

$$\rho u C_p T(2\pi r)\Delta r \,|_x - e_{out} = \rho u C_p T(2\pi r)\Delta r \,|_{x+\Delta x} = q_w(2\pi r)\Delta x - q_c(2\pi r)\Delta x$$

For $2\pi\rho ur = \dot{m}$ and dividing by Δx and taking the limit of Δx to 0, we obtain

$$\frac{d\dot{m}C_p T}{dx} = (q_c - q_w)\,2\pi r$$

where $q_c = h_c A\,(T_{aw} - T_{co})$ and $q_w = h_w A\,(T_{co} - T_w)$

$$\frac{\dot{m}C_p}{2\pi r}\frac{d\dot{m}C_p T}{dx} = -\alpha T_b + \beta$$

Here, $\alpha = h_g + h_r$ and $\beta = h_g T_{aw} + h_r T_w$. After integrating from x = 0 to x = L and for T = T_{in} to T_{out}, we obtain the following relation:

$$T_{out} = \frac{\beta}{\alpha} + \left(T_{in} - \frac{\beta}{\alpha}\right) e^{-\frac{2\pi RL\alpha}{\dot{m}C_p}}$$

This equation relates the geometry, mass flow rate, and inlet/outlet temperatures which can approximate the mass flow required for film cooling, critical boil-off length, or the temperature at a specific station.

From the derivation of the governing equations, a MATLAB script was composed to estimate the temperature along the entire rocket chamber with the given design constraints. From there we can predict the film coolant temperature at each station of the engine. The temperature is numerically integrated along the chamber stations taking into the changing thermophysical properties of RP1. The output of the MATLAB script is shown figure 12. With the film coolant acting as an isothermal sink, the chamber walls are kept cool and the predicted max of 635K is within the CCT. The result is similar compared to that of RPA's output. With an additional margin, it was determined that an RP1 film cooling of 13% total mass flow is satisfactory for cooling.

The script also yields the fluid dynamics information in the regen channel: Reynolds number, maximum velocity, and head loss, regen tubular diameter. This information can be used to check variables values are within constraint.

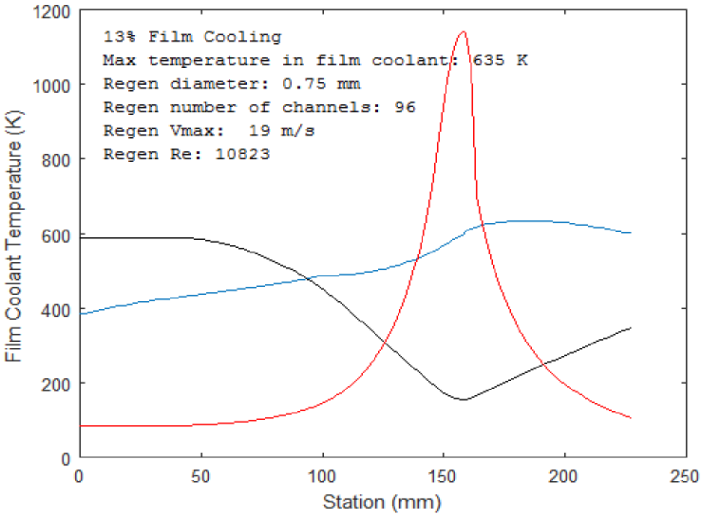

Figure 12 - Film Coolant Temperature as a function of the position in the engine
*Engine Contour (**black**), heat flux coefficient (**red**), and film coolant temperature (**blue**)*

CFD Analysis

A CFD analysis was conducted using ANSYS Fluent on the regenerative cooling jacket to determine the headloss that our RP-1 experiences while travelling through the coolant channels. In order to simplify the process, a single coolant channel was isolated downstream of the lower coolant ring, and thus it was assumed that the lower manifold creates a uniform pressure profile at the inlet of each channel. The channel was meshed rather simplistically by setting mesh relevance to 0 and allowing Fluent to create an unstructured tetrahedral mesh. A standard k-omega turbulence model was selected due to its wide range of industrial applications and its performance with high pressure gradient flow. The density and dynamic viscosity values for RP-1 were used to define a new working fluid to be used in the Fluent solver.

Two boundary conditions are necessary to compute the pressure drop across the coolant channel. At the inlet, we have a mass flow boundary condition, dictated by the amount of fuel mass flow we want being injected into our engine. To find the mass flow through a single coolant channel, the mass flow of the entire system was divided by the number of coolant channels, 95. At the outlet, a pressure boundary condition was set at 700 psi, an estimate of the pressure we expect at the top of the coolant channels that was determined by working backwards from our estimated 500 psi chamber pressure and $\Delta p_{inj.} = 0.3 p_c$ and assumed losses in the injector face. With these conditions, the following pressure profile was generated.

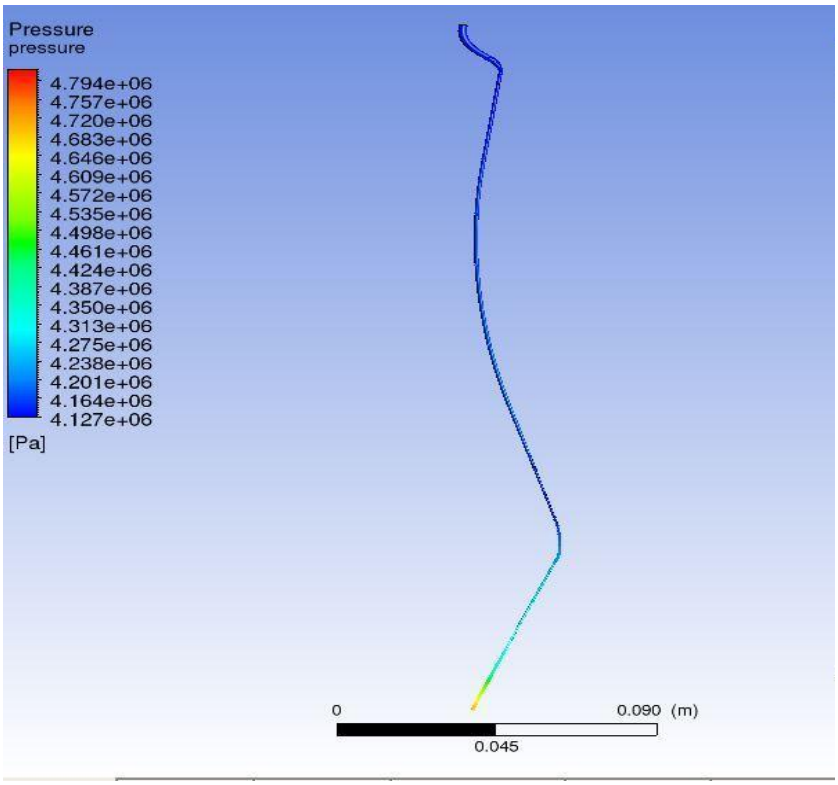

Figure 13 - Pressure contour for Ignus 2.0 coolant channel

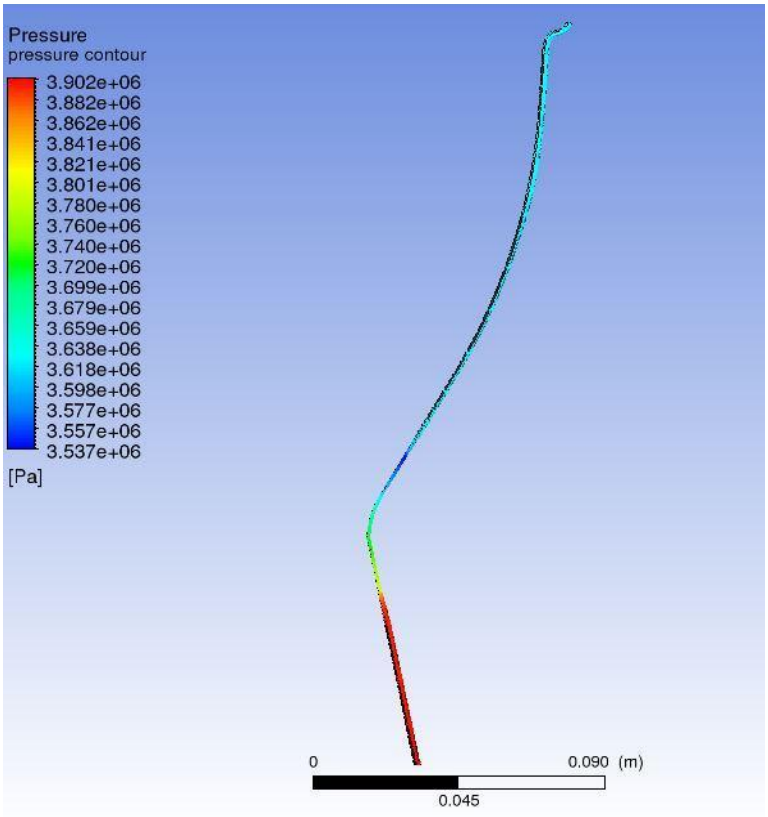

Figure 14 - Pressure contour for Ignus 1.0 coolant channel

The simulation found that we will experience a pressure drop of approximately 80 psi, with the vast majority of the head loss occurring below the nozzle throat where the channels are at their thinnest. A similar simulation was conducted on the Ignus 1.0 engine geometry shown on the following page.

These results correspond to a head loss of 50-60 psi. The increase in head loss in the Ignus 2 engine is due to the variable channel diameter of our coolant channels and their relative thinness. While the head loss is greater In Ignus 2, we expect the coolant channels to operate more effectively and prevent the chamber burnthrough that was observed in Ignus 1. Thin coolant channels increase fluid velocity around the throat and allow more heat to be drawn out of the chamber.

Data Acquisition (DAQ)

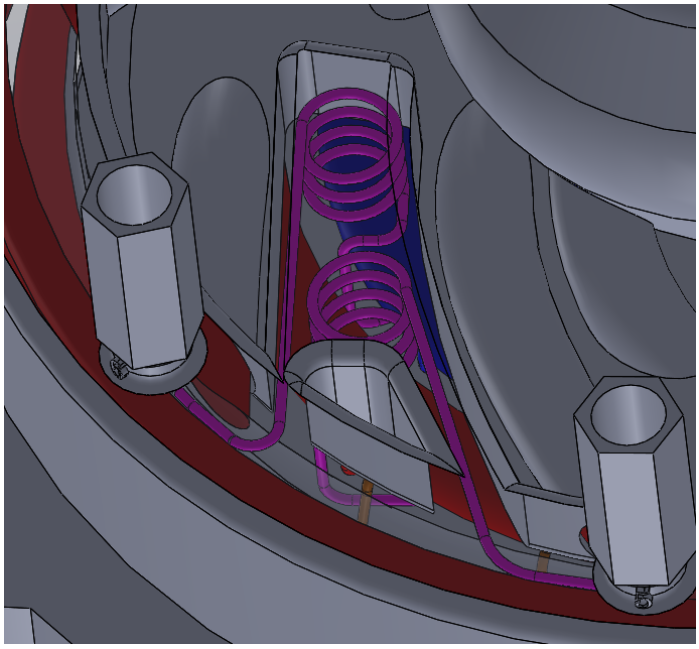

Figure 15 - Helical coils for Pressure Transducers

Similar to the Ignus 1.0 engine, additive manufacturing allows for the integration of instrument ports to decrease the chance for plumbing errors and overall manufacturing complexity. These ports allow for the implementation of pressure transducers to obtain data from feature locations. Helical coils were designed to stagnate the fluid pressure readings, each with a line length of over 6 inches. The lengthy service lines create a cushion of air between the fluids and the transducers.

In addition to the pressure transducers, thermocouples will be placed on the injector plate and combustion chamber. Figure 16 illustrates the location of the thermocouples.

In the event of an emergency shut down for when the temperature of the combustion chamber walls reach 80% of the melting point of Inconel, the information from the TCs will relay to the test stand to shut off the main line propellant valves.

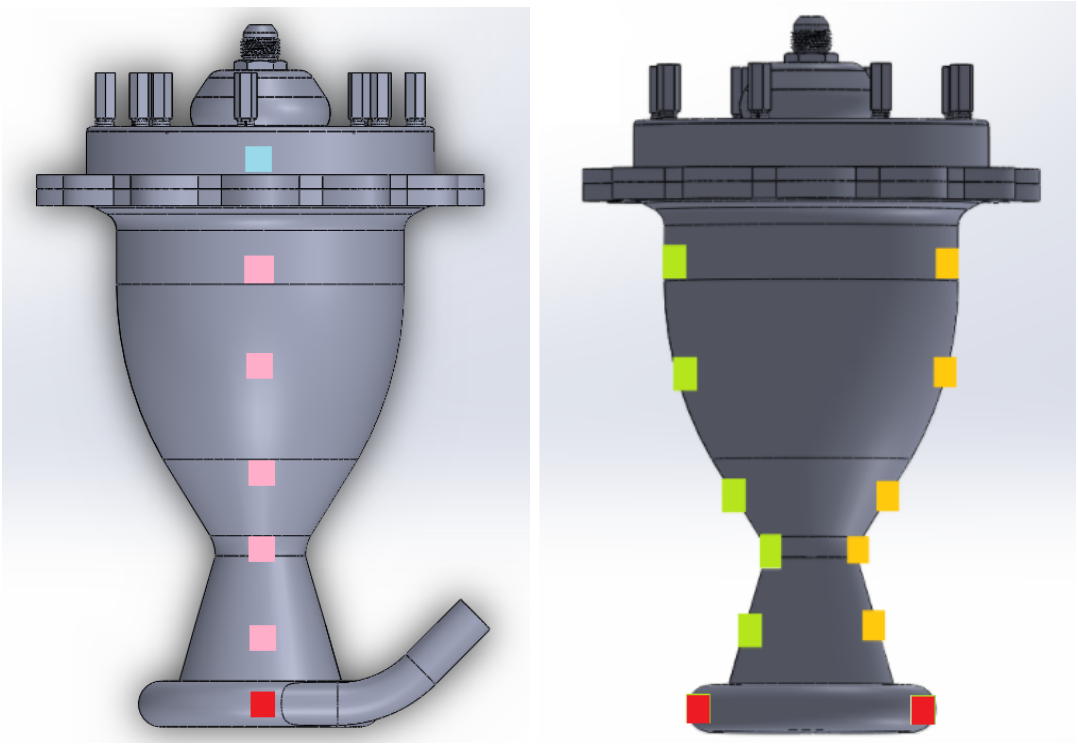

Figure 16 - Placements of TCs
The pink, green, and yellow TC locations are 120° from each other along the combustion wall
The red TC locations are 120° from each other on the inlet fuel plenum
The cyan TC location is on the fuel annulus

The pressure transducers of choice are PCB Piezotronics Model 113B24 ICP Pressure Sensors. These dynamic pressure sensors are designed for shock tube and blast wave measurements and for high frequency applications. The 8 pressure transducers measure pressure in the internal manifold, combustion chamber, and propellant plenums.

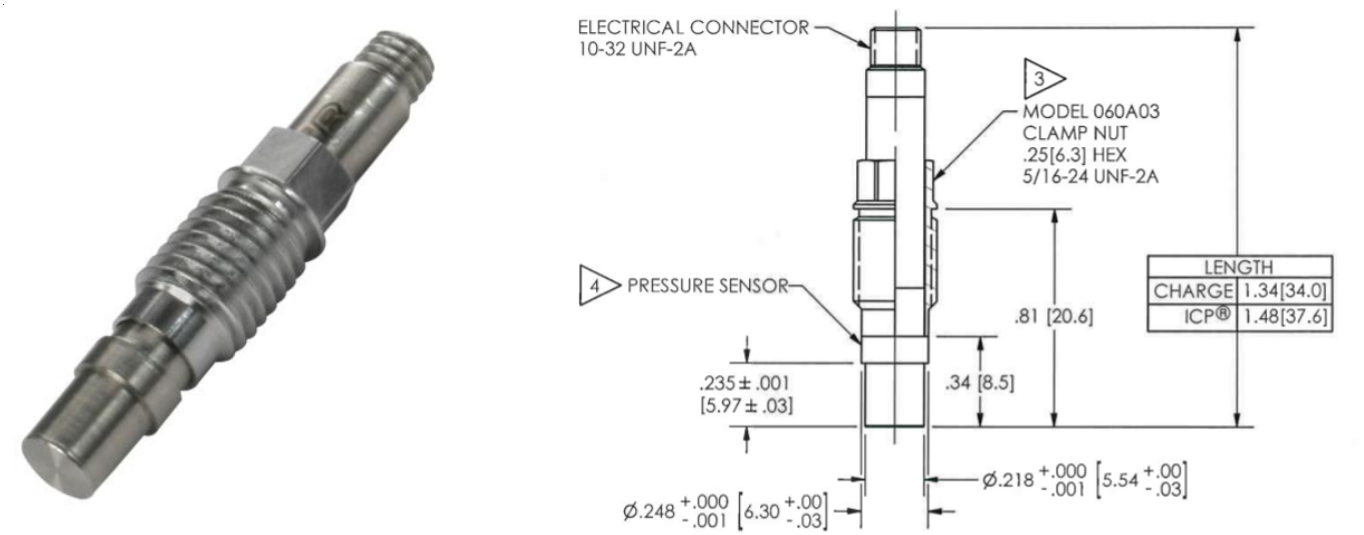

Figure 17 - Pressure Transducer and Engineering Drawing

Appendix

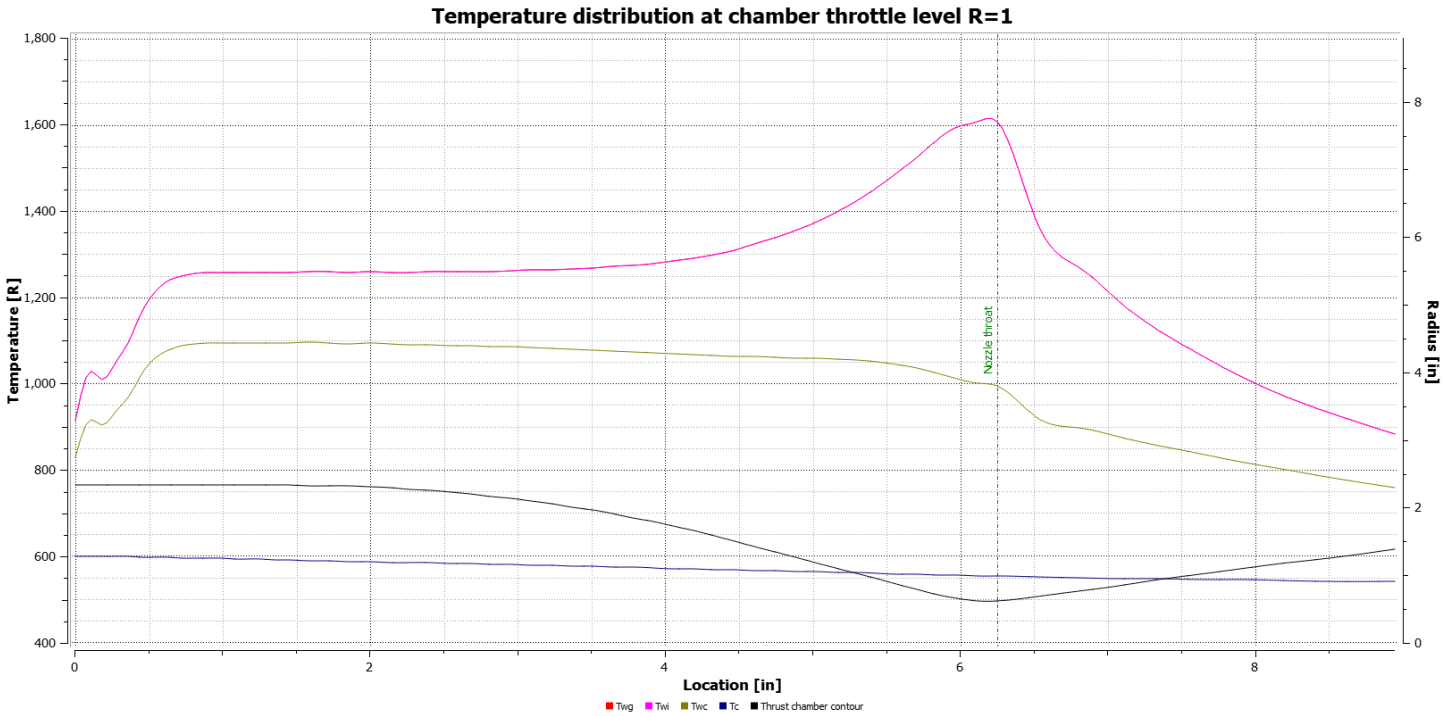

T_{wg} - T_{wi} - T_{wc} - T_c - Thrust Chamber Contour

Appendix 1 - Temperature Distribution Along Engine Contour

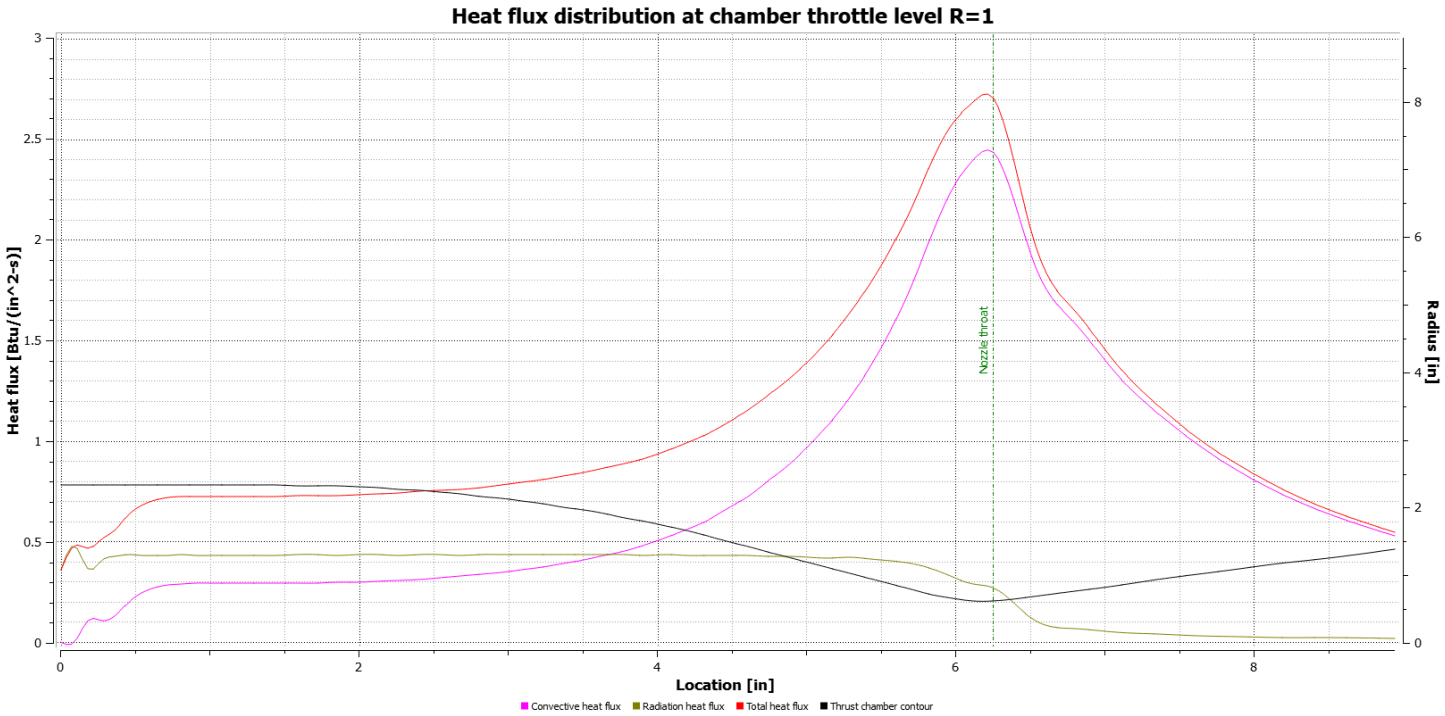

T_{wg} - T_{wi} - T_{wc} - T_c - *Thrust Chamber Contour*

Appendix 2 - Heat Flux Distribution Along Engine Contour

Material Properties

Thermal Conductivity (W/m/K)	Temperature (K)
10.31	293
11.88	373
13.6	473
16.6	673
20.1	873
26.3	1073
30.75	1573

Table 3. Temperature dependence of specific heat capacity for Inconel 718.

Specific Heat Capacity (J/kg·K)	Temperature (K)
362	293
378	373
400	473
412	673
460	873
1073	1073
1573	1573

Table 4. Inconel 718 physical properties.

Density (kg/m^3)	Poisson Ratio	Modulus of Elasticity—293 K—(Gpa)
8300	0.3	217

Appendix 3- Material Properties of Inconel 718

Substance	Formula	Melting temp. T_f K	Boiling temp. T_b K	Melting enthalpy h_{sl} kJ/kg	Boiling enthalpy h_{lv} kJ/kg	Density (mass) ρ kg/m³	Thermal expansion $\alpha \cdot 10^6$ K⁻¹	Compressibility[a] $\kappa \cdot 10^9$ Pa⁻¹	Surface tension[b] σ N/m	Thermal capacity c_p J/(kg·K)	Thermal conductivity k W/(m·K)	Dynamic viscosity $\mu \cdot 10^6$ Pa·s
Kerosene, Jet A-1, RP1	($C_{12}H_{24}$)	230[g]	450[g]		250	820	830	0.70	0.028	2000	0.13	2400

Appendix 4 -Inconel 718 Thermal Conductivity

References

Atyam, Deepak M., and Ngoc. H. Nguyen. *Designing and Testing Liquid Engines for Additive Manufacturing*. AIAA Paper. 2014.

Gill, G. S., and W. H. Nurrick. *Liquid Rocket Engine Injectors*. NASA SP-8089, 1976.

Huzel, Dieter K., and David H. Huang., *Modern Engineering for Design of Liquid Propellant Rocket Engines,* 2nd ed., AIAA, Washington DC, 1971.

Inch Fastener Standards, 7th ed. 2003. B-8

"Inconel Alloy 718" Special Metals. Web. 2007.

Sutton, George P., and Oscar Biblarz. *Rocket Propulsion Elements*. 8th ed. John Wiley & Sons, 2001. Print.

Turner, M. J., Martin, H. C., and Leible, R. C., "Further Development and Applications of Stiffness Method," *Matrix Methods of Structural Analysis*, 1st ed., Vol. 1, Wiley, New York, 1963.